Available online at www.sciencedirect.com

ScienceDirect

Energy Procedia 137 (2017) 100–107

Energy Procedia

www.elsevier.com/locate/procedia

14th Deep Sea Offshore Wind R&D Conference, EERA DeepWind'2017, 18-20 January 2017, Trondheim, Norway

A New Foundation Model for Integrated Analyses of Monopile-based Offshore Wind Turbines

Ana M. Page[a,b*], Kristoffer Skjolden Skau[a,b], Hans Petter Jostad[a,b], Gudmund Reidar Eiksund[a]

[a]*Department of Civil and Environmental Engineering, NTNU, Høgskoleringen 7A, 7491 Trondheim, Norway*
[b]*Norwegian Geotechnical Institute, Sognsveien 72, 0855 Oslo, Norway*

Abstract

Offshore wind turbines are highly dynamic and tightly coupled systems subjected to variable cyclic loads. Designing and optimizing the support structure is a complex task, where several load scenarios have to be analysed to account for the various uncertainties. Improving the accuracy of analysis tools used in the design and optimization process can increase the reliability and thus reduce uncertainties and risks. For monopiles supporting offshore wind turbines, the current design practice is to model the foundation response by API *p-y* curves. Discrepancies between the assumptions considered in the API *p-y* curves and the actual pile behaviour have been extensively identified in the literature, and their applicability to predict pile behaviour in integrated analyses of offshore wind turbines has been questioned. This paper presents a new foundation model for integrated analyses of monopile-based offshore wind turbines. The model is simple and hence computational efficient, but still able to reproduce key characteristic in monopile foundation behaviour that are not accounted for in the current modelling approach. The model input is based on finite element analyses of the soil and the foundation, which makes it possible to calibrate the model to different soil conditions. The basic features of the model are described and its limitations are discussed. The performance of the new foundation model is demonstrated for time histories that are representative for an offshore wind turbine and compared with the response from API *p-y* curves. In contrast to the API *p-y* curves, the new model can reproduce different foundation stiffness for unloading and reloading and foundation damping depending on the loading history, which is observed in real pile behaviour. A more realistic foundation modelling will lead to more accurate predicted loads, reduced uncertainties in the estimated fatigue lifetime and therefore reduced risk in the design.

Peer-review under responsibility of SINTEF Energi AS.

Keywords: Offshore wind turbines; fatigue design; soil-pile interaction; *p-y* curves; foundation modelling; macro-element model;

1. Introduction

Offshore wind turbines (OWTs) are complex systems subjected to a significant source of quasiperiodic excitation from wind and waves. Fatigue is often the governing factor for the support structure design and therefore dynamic structural analyses are mandatory for an accurate fatigue assessment. Dynamic structural analysis is based on integrated load simulations of several design load cases [1] and they are generally performed in the time-domain [2]. An integrated load simulation or integrated analysis of an OWT refers to the analysis of an entire OWT (i.e. RNA, support structure, and foundation) under combined aerodynamic and hydrodynamic loading and requires numerical models for all parts of the OWT. The numerical modelling of the foundation is an essential part for the integrated model of the OWT due to its impact on the global dynamics. Variations in the foundation stiffness

* Ana M. Page. Tel.: +47-406-983-28; fax: +47-222-304-48.
E-mail address: ana.risueno@ntnu.no

1876-6102
Peer-review under responsibility of SINTEF Energi AS.
10.1016/j.egypro.2017.10.337

lead to significant changes in the natural frequencies of the OWT. This can bring the natural frequencies of the structure closer to excitation frequencies, increasing the fatigue damage and consequently reducing the intended fatigue lifetime [3]. An accurate predicted foundation stiffness is therefore important for a correct estimation of the fatigue lifetime. In addition, the damping contribution from the foundation helps to attenuate the dynamic amplification of the response, especially during idling conditions when aerodynamic damping is relatively small.

1.1. Monopile foundation behaviour

An accurate foundation model should be able to reproduce the main characteristics of the foundation behaviour for the loads acting on OWTs. Among the different concepts for OWTs support structures, the monopile is a preferred solution for shallow and intermediate water depths, accounting for approximately 75% of installed support structures. Piles supporting monopile-based OWTs are subjected to large horizontal loads which result in large overturning moments at mudline. In comparison, the applied vertical load is relatively small [4]. Large diameter piles resist these loads by mobilizing lateral resistance in the soil. Due to the interaction between the pile and the soil, the following characteristics are observed:

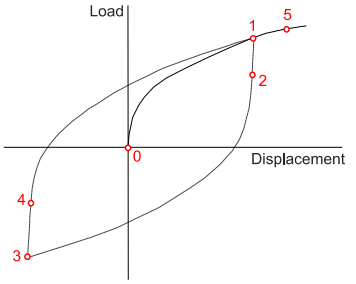

Fig. 1. Illustration of the non-linear hysteretic pile foundation response.

(1) *Non-linear load-displacement response*. Piled foundations exhibit a non-linear response during lateral loading, due to the non-linear soil behavior, as illustrated in Fig. 1 between points 0 and 1.

(2) *Hysteretic behaviour*. When the load acting on the foundation is reversed (points 1 to 2 in Fig. 1), the soil around the pile is unloaded. Initially the soil unloading is elastic and the pile response is stiffer than prior to the reversal. As the magnitude of the load reversal increases, plastic deformations are generated and the stiffness decreases (points 2 to 3). During reloading (points from 3 to 1 through 4), a similar pattern is observed. This behaviour generates a hysteretic loss of energy (area enclosed in the loop 1-2-3-4-1), which can be translated to a hysteretic damping at foundation level. In addition, foundations also dissipate energy by geometric spreading of the waves propagating through the soil. This type of energy dissipation, also known as radiation damping, depends on the loading frequency, and it is negligible for frequencies below 1 Hz [5]. For monopiles supporting OWTs, radiation damping can be neglected, and the main foundation damping contribution comes from hysteretic damping.

Full-scale measurements of monopile-based OWTs also confirm the non-linear hysteretic foundation response. Kallehave et al. [6] observed that the measured natural frequency of monopile-based OWTs decreased with increasing wind speeds, and related it to increasing displacement levels. The same conclusion was reached by Damgaard et al. [7] when analysing the reduction in natural frequency with increasing acceleration levels. Foundation damping values between 0.25-1.5 % of critical damping have been found in several studies under different loading conditions and for different soil profiles [7-10]. In addition to the described behaviour, pile foundations can also exhibit soil degradation, pore pressure build-up, ratcheting, gapping and density changes due to cyclic loading. These effects are expected to be negligible at the load levels considered in the fatigue analyses design and for the relatively few number of cycles present in the 10 to 60 minutes long simulations. However, they might be relevant if higher load levels are considered.

1.2. Current foundation modelling in integrated analyses

The most common approach for modelling the foundation response in integrated analyses is the so-called *p-y* curve approach, where the pile is modelled as a beam and the soil is represented as a series of discrete, uncoupled, non-linear elastic springs at nodal points along the pile. The springs relate the local lateral resistance, p, to the local lateral displacement of the pile, y. The DNV standard [2] recommends the use of API *p-y* curve formulation [11] for the estimation of the lateral pile capacity. Discrepancies between the assumptions considered in the API formulation and the actual pile behaviour have been extensively identified in the literature [12, 13]; and their applicability to predict pile behaviour in integrated analyses of OWTs has been questioned. The most relevant shortcomings while modelling pile behaviour in integrated analyses of OWTs are:

(1) *Different pile geometry and loading conditions*. The API methodology was developed and validated on slender small diameter piles (from 0.5 to 1.3 m) with length to diameter ratios higher than 20, subjected static loads with low lateral-to-vertical load ratios and small overturning moments [14]. In contrast, piles supporting OWTs typically present pile diameters in the range of 4-7.5 m and penetrate to a depth of 15-30 m below mudline, resulting in depth to diameter ratios around 2-6. They are subjected to large amplitude-variable cyclic horizontal loads and moments at mudline, as illustrated in Fig. 2. Under these conditions, piles show quite a rigid behaviour, and the contribution of some components of soil resistance, like the side and base shear, may be relevant [15]. These components are not included in the API *p-y* formulation, which may lead to an inaccurate prediction of the pile response.

(2) *Lack of an accurate prediction of the foundation stiffness and foundation damping*. The API *p-y* curves were formulated with focus on providing a conservative ultimate pile capacity rather than precise foundation stiffness, and they fail to accurately reproduce the initial lateral pile stiffness. The formulation provides only two *p-y* curve functions: one for sand and one for clay. Stress-strain curves for soils show a much greater variety, impossible to describe by only two functions. In addition, API *p-y* curves are non-linear elastic, which means that hysteretic damping is not included

Besides these shortcomings, comparison between designed and measured fundamental frequencies from OWTs supported by monopiles reveals that the fundamental frequencies are generally underestimated in the design [16, 17]. Zaaijer [17], Hald et al. [18] and Kallehave et al. [6] indicated that this is consistent with the notion that the API *p-y* formulation for piles in sand tends to underestimate the soil stiffness.

1.3. Alternative p-y models for integrated load simulations

Given the limitations of the API *p-y* curves in integrated analyses of OWTs, alternative formulations have been proposed, such as *p-y* curves extracted from FE analysis of the soil-foundation system or extensions of the *p-y* approach where all the components of soil resistance are included [15]. Despite that these curves capture the pile stiffness more accurately, most of them are still elastic, which means that the foundation hysteretic damping is not modelled. To address this issue, Hededal and Klinkvort [19] introduced elasto-plastic springs. This model can produce hysteretic damping, however, the non-linear load response is modelled in a simplistic manner. A more realistic foundation response based on the combination of API *p-y* curves and Masing's rule [20] is suggested by Beuckelaers [21]. However, the contribution of some components of soil resistance such as side and base shear, which might be relevant for monopile-based OWT, are ignored in the methodology.

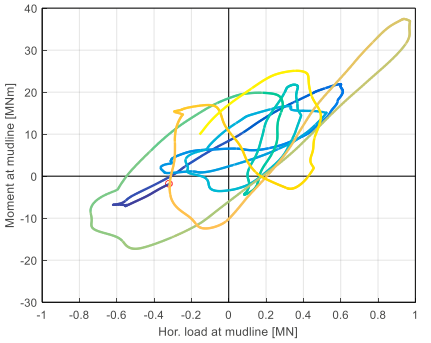

Fig. 2. Simulated horizontal load and overturning moment at mudline from an idling monopile-based OWT subjected to a turbulent wind speed of 26 m/s.

1.4. Full 3D continuum modelling of soil

Full 3D continuum modelling of the soil volume by FEA would be the most accurate and flexible modelling approach. In this type of analyses, the soil is described by constitutive models, which are based on element testing and material laws. Constitutive models can describe the soil response more realistically than *p-y* curves. In addition, FEA can capture effects of stress re-distributions along the pile and interactions between soil layers with different behaviour. The main disadvantage is the large computational cost of time-domain 3D FEA with continuum elements, which makes the approach impractical for integrated analyses in the design process.

1.5. Macro-element foundation models

An alternative to relatively simple *p-y* models and to the computationally expensive continuum FEA of the soil and the foundation is the model approach referred to as macro-element modelling. These models reduce the foundation and the surrounding soil to a force–displacement relation in one point at an interface separating the foundation and the rest of the structure, typically located at mudline. The response of this point is determined by the behaviour of pile and soil below mudline, but these are not included explicitly in the model.

The idea behind the macro-element concept for foundations was initially presented by Roscoe and Schofield [22]. The first macro-element models only considered flat footings and spudcans foundations [23-25]. The concept has later been extended to skirted foundations [26] and to pile foundations [27-29]. Most macro-element models base their formulation in FEA or in model testing. Modeling of piled foundations with a macro element model has some advantages compared to the *p-y* curve approach. First, fewer degrees of freedom are required in integrated analyses than for distributed *p-y* curves. This opens up for employing more complex models without increasing the overall computational cost. Second, for some conditions, it is easier to accurately describe the overall response of a pile rather than accurately describe the varying soil or *p-y* response along it. This is especially relevant for dynamic structural analyses, where the aim is to describe the dynamic system as accurate as possible. The model presented in this paper belongs to the family of macro-element models.

2. Finite Element Analyses to serve as a basis for the model formulation

Finite Element Analyses of the soil volume and the foundation have been performed for different soil profiles and load combinations with the commercial software PLAXIS 3D. In this section, one of the cases is selected and its results are presented. The case consists of 6 m diameter steel pile, with a wall thickness of 0.06 m, embedded 36 m in a homogeneous clay profile. The soil properties are listed in Table 1 and the finite element model is shown in Fig. 3. Roller boundaries are applied at the vertical boundaries of the finite element model, and fixed boundaries are applied at the bottom. The pile is assumed to have linear elastic behavior, while the soil is represented with the NGI-ADP [30] soil model, which has a non-linear stress path dependent behavior typical for clays. The contact between the soil and the pile is modelled by an interface, which has the same stiffness as the soil and half of its strength. A horizontal load H and a moment M are applied on the pile's cross-section at mudline. Load-controlled analyses are performed for different M/H ratios. The relation between the applied loads and the response of the foundation and the surrounding soil is evaluated by analyzing the computed horizontal pile displacement u and pile rotation θ at mudline.

Table 1. Parameters of the soil profile considered in the selected case

Parameter	Nomenclature	Value	Unit
Unit weight of the soil	γ	18	kN/m^3
Normalized initial shear modulus	G_{max}/s_u	500.0	-
Undrained shear strength at mudline	s_u	0.1	kPa
Increase of undrained shear strength with depth	$\Delta s_u/z$	13.9	kPa/m
Shear strain at failure in compression	γ_f^C	0.1	-
Shear strain at failure in DSS and extension	γ_f^{DSS}, γ_f^E	0.15	-

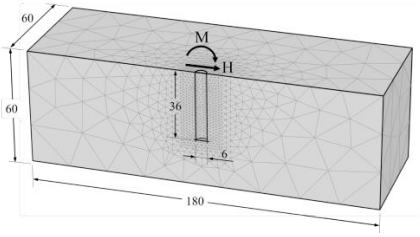

Fig. 3. Finite Element model of the soil and the foundation

The total horizontal displacement u and the total rotation θ at mudline computed by finite element analyses are plotted in Fig 4, together with an interpolated surface. To ease the visualization of results and the formulation of the model, the global response is divided into an elastic and a plastic response. As expected, the flat shape of the interpolated elastic response indicates that the elastic horizontal displacement u_e and the elastic rotation θ_e can be expressed as a linear relation between H and M, i.e. through an elastic stiffness matrix.

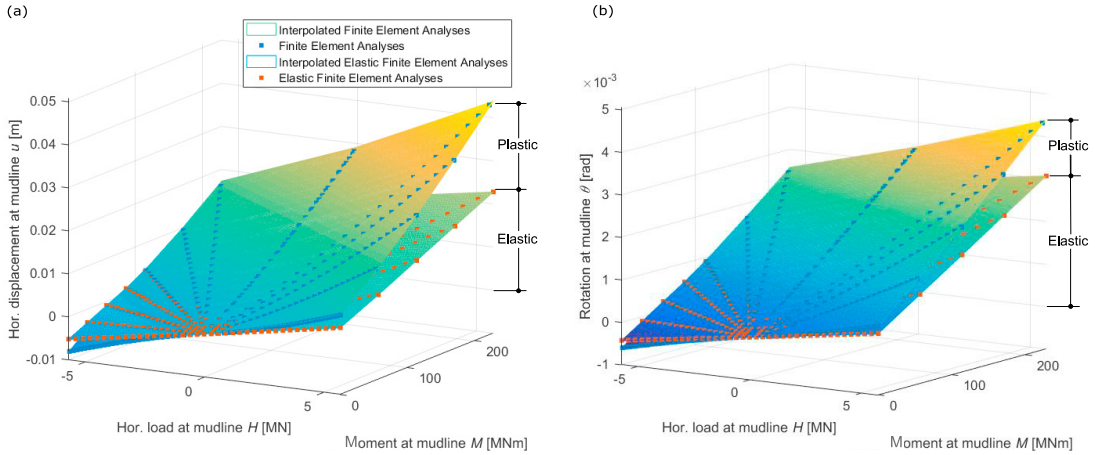

Fig. 4. Total and elastic response computed by FEA as a function of the horizontal load and an overturning moment at mudline, and linearly interpolated surfaces: (a) horizontal displacement at mudline; (b) rotation at mudline. The difference between the total and the elastic response is the plastic response.

The relation between the plastic horizontal displacement u_p and plastic rotation θ_p at mudline as a function of H and M is not linear and makes the elasto-plastic surface in Fig 4 curved. The plastic displacements u_p and θ_p at mudline can also be seen in the contours presented in Fig 6a. For both the plastic horizontal displacement and the plastic rotation, the contours are approximately parallel straight lines. The distance between contours decreases with increasing M and H, which is expected in a non-linear model. To simplify the contours, the response can be evaluated at a certain depth L_β below mudline, at a point denoted the plastic decoupling point. The response at the plastic decoupling point is related to the response at mudline by assuming equilibrium of forces (Fig. 5a) and rigid body movement (Fig. 5b and Fig. 5c). The distance L_β is defined as the ratio between the plastic horizontal displacement u_p and the plastic rotation θ_p at mudline, i.e. $L_\beta = u_p / \theta_p$. For small rotations this implies that the plastic horizontal displacement at the plastic decoupling point is zero ($u'_p = u_p - \theta_p \cdot L_\beta = 0$). For the load levels considered in this study, L_β is approximately constant. For higher loads, it is expected that L_β will increase.

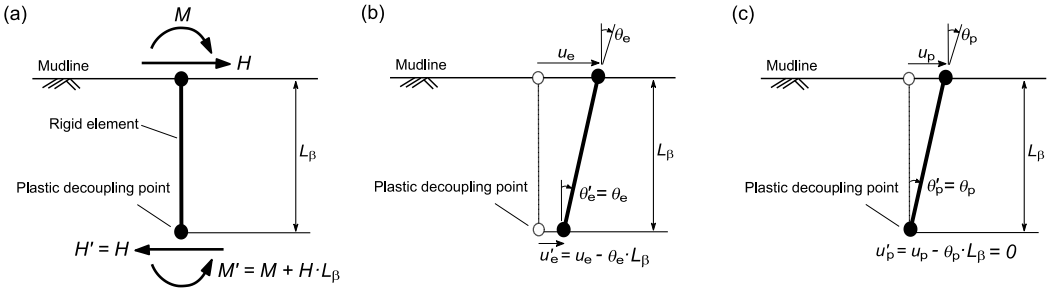

Fig.5. Relations between mudline and the plastic decoupling point: (a) horizontal force and overturning moment; (b) elastic horizontal displacement and rotation; (c) plastic horizontal displacement and rotation.

By changing the reference depth, the contours presented in Fig. 6a are transformed into the contours in Fig. 6b. The contours in Fig. 6b confirm that the horizontal plastic displacement is very close to zero and that the plastic rotation contours are parallel to the horizontal axis. This indicates that the plastic rotation θ'_p is independent of the horizontal force H' at this point. Therefore, the relation between the plastic displacements (horizontal displacement and rotation) and load (horizontal load and moment) can be reduced to a 1D relation between the plastic rotation θ'_p and the moment M' at the plastic decoupling point. The M' - θ'_p relation can be reproduced with a 1D elasto-plastic model. The elastic response has a different decoupling depth but since the only transformation is a change in the coordinate system, the elastic response can still be described by an elastic flexibility matrix at the plastic decoupling point.

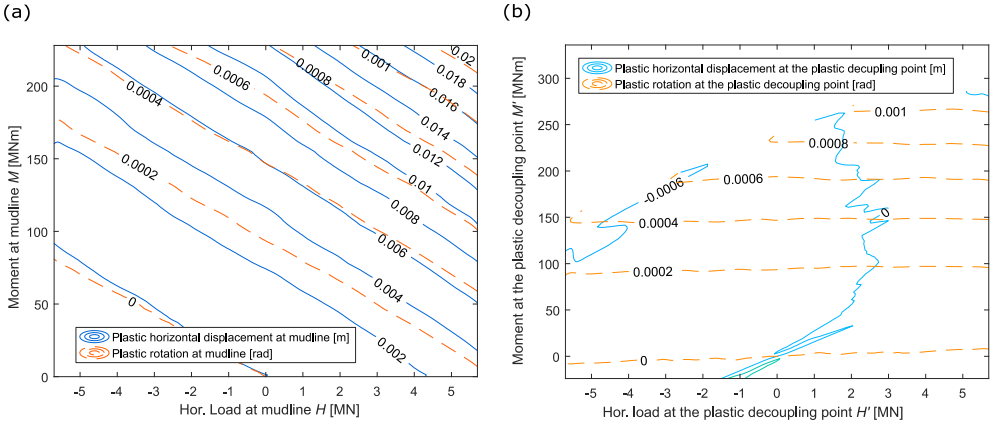

Fig. 6. Contours of plastic horizontal displacement and plastic rotation as a function of the horizontal load and the moment: (a) at mudline; (b) at the plastic decoupling point. By plotting the results at the plastic decoupling point, the 2 degrees-of-freedom force-displacement relation at mudline can be simplified to a 1 degree-of-freedom system.

3. A new macro-element model for integrated analyses of monopile-based offshore wind turbines

3.1. Formulation of the macro-element model

The macro-element model relates the loads (horizontal load and the overturning moment) to the displacements (horizontal displacement and the rotation) at mudline. Based on the results from FEA, a simple but effective modelling framework for monopile response has been developed. The framework has a well-defined physical analogy, it is easy to implement and captures some of the key characteristics identified from the FEA results. The finite element analyses indicate that the model can be simplified by working out the formulation at the plastic decoupling point. At this point it can be assumed that only plastic rotations are generated, i.e. $u'_p = 0$, and that the plastic rotation θ'_p is a function of the overturning moment M' only, which means that $\theta'_p(H') = 0$. The application of a horizontal load H' and an overturning moment M' at the plastic decoupling point generates a horizontal displacement u' and a rotation θ' as follows:

$$\begin{aligned} u' &= u'_e + u'_p = u'_e(H') + u'_e(M') \\ \theta' &= \theta'_e + \theta'_p = \theta'_e(H') + \theta'_e(M') + \theta'_p(M') = \theta'_e(H') + \theta'_{M'}(M') \end{aligned} \tag{1}$$

From the terms presented in Eq. 1, $u'_e(H')$, $u'_e(M')$ and $\theta'_e(H')$ are elastic and can be calculated from H' and M' using an elastic stiffness matrix. The relation between $\theta'_{M'}(M')$ and M' is elasto-plastic, and can be reproduced by using a 1D IWAN kinematic hardening model [30], which provides a non-linear moment-rotation curve and can reproduce hysteretic behaviour.

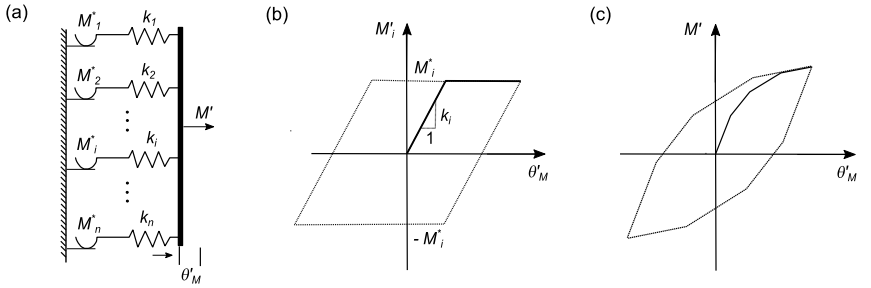

Fig. 7. 1D kinematic hardening model: (a) physical representation; (b) moment-rotation behaviour of each spring and slip element; (c) resulting moment-rotation behaviour of all the parallel coupled springs and slip elements.

The 1D kinematic hardening model consists of a series of springs and slip elements coupled in parallel as illustrated in Fig 7a. Each of the elastic springs, with a stiffness k_i, is coupled in series with a slip element with a critical slipping moment M^*_i. All the springs are subjected to the same rotation $\theta'_{M'}$. The linear elastic-perfectly plastic behavior of each individual spring and slip element is shown in Fig. 7b. Each moment M'_i increases linearly with a stiffness k_i until the critical slipping moment M^*_i is reached. When the loading direction is reversed, each spring and slider element unloads or reloads following the spring stiffness k_i, reproducing Masing's rule [20]. The moment M' is calculated as the sum of each M'_i. The model gives a stepwise variable stiffness and an overall kinematic hardening behavior when subjected to cyclic loading. An example of the θ'_M and M' response is shown in Fig. 7c. With sufficient number of spring elements included in the model, the $\theta'_{M'}$ and M' response becomes smooth. An advantage of the IWAN modelling approach is the flexibility to describe very different shapes of the moment – rotation curve, which makes this model applicable to foundation problems with different types of soil behaviour.

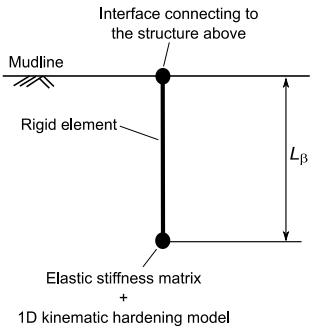

Fig. 8. Structure of the macro-element model.

The macro-element is then composed of a rigid element connecting the structure-foundation interface node at mudline with the plastic decoupling point, an elastic stiffness matrix and a 1D kinematic hardening model, as sketched in Fig. 8.

3.2. Implementation and calibration of the macro-element model

The foundation model is being implemented in the OWT simulation code *3DFloat* [32] via a *dll* interface. In each calculation step, *3DFloat* passes on three displacements and three rotations at mudline to the foundation model, which transfers back three forces and three moments. The relation between the horizontal displacement and rotation and between the horizontal force and moment at mudline in the main wind direction is non-linear and it is computed by the macro-element model. The relation between the forces and displacements in the out of plane directions is linear elastic.

The calibration of the foundation model requires two types of input: (1) the coefficients of the elastic stiffness matrix and (2) a table containing the moment, horizontal displacement and rotation at mudline from non-linear analyses with $H = 0$. The elastic stiffness matrix coefficients can be obtained from FEA, by modelling the soil as a linear elastic material, or by using well-established semi-empirical formulas for different pile geometries and soil types [33, 34]. The table with the moment, horizontal displacement and rotation at mudline, can be obtained from static pushover FEA with a soil model that represents the relevant cyclic nonlinear response. Reference is made to [35-37] for more information regarding the use of FEA to compute cyclic foundation response based on soil element behavior.

3.3. Verification of the macro-element model

The verification of the macro-element model implementation is assessed by comparing the results of the macro-element model with FEA results of the soil volume and the foundation. The finite element model employed in the calculations is shown in Fig. 3.

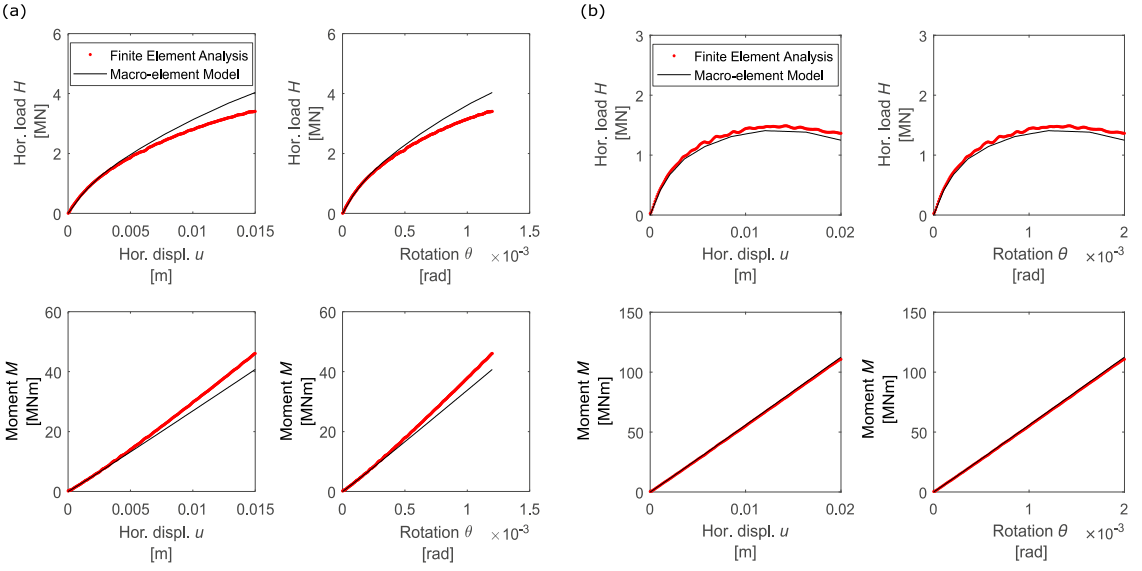

Fig. 9. Verification of the macro-element model implementation. Comparison between the FEA and the macro-element model results: (a) for a monotonic test with $u/\theta = 12.5$, which leads to a high H and a relatively low M load path; (b) for a monotonic test with $u/\theta = 10$, which leads to a relatively constant H and high M load path.

In the comparison, a 6 m diameter steel pile with a wall thickness of 0.06 m is embedded 36 m in a homogeneous clay profile. The clay is characterised with a constant undrained shear strength with depth of 50 kPa, a normalized initial shear modulus of 500, a shear strain at failure in compression of 0.10 and shear strain at failure in direct simple shear (DSS) and extension of 0.15. Input to the macro-element model are an elastic foundation stiffness matrix and a table containing the moment, horizontal displacement and rotation at mudline from a static FEA with $H = 0$. The NGI-ADP model [29] is employed to describe the clay behaviour in the FEA. Two displacement-controlled monotonic increasing tests have been evaluated: one with $u/\theta = 12.5$ and the other with $u/\theta = 10$.

Good agreement is found between the macro-element results and the finite element results for low horizontal load levels, as shown in Fig. 9b. This indicates that the implementation of the macro-element model is correct and that the simple macro-element model is capable of reproducing, for the given example and under the load levels considered, the response from the more advanced FEA. However, in the test with a larger horizontal load (Fig. 9a), a poorer agreement is found. This is due to the plastic decoupling moving deeper for higher loads in the FEA while defined constant in the macro-element model.

4. Comparison with API *p-y* model response

The macro-element model calibrated by FEA has been compared with API *p-y* curves for the case described in Section 2. Two loading conditions have been analysed: case 1 illustrates a loading path that could correspond to some seconds of an idling situation, and case 2 could represent some few cycles of a rotor stop test. The horizontal load vs. rotation curve computed with the macro-element model calibrated by FEA and with API *p-y* curves are presented in Fig. 10. These curves illustrate the capability of the macro-element model to reproduce different foundation stiffness after load reversals and hysteretic damping. During monotonic loading, e.g. stretch A-D-E in case 1, a similar path is followed both in the macro-element model and in API *p-y* curves, with the macro-element model calibrated from FEA providing higher stiffness around point A. However during load reversals, e.g. stretch E-F-G in case 1, the computed response differs. On one hand, the macro-element model provides a higher stiffness at the reversal point E, which gradually decreases until F. After the load reversal in F, the stiffness increases and the symmetric behaviour is followed until G. The area enclosed in the loop E-F-G dissipates some energy, leading to hysteretic foundation damping. This response mimics the behaviour observed in pile tests. On the other hand, with API *p-y* curves, the same elastic curve is followed in the stretch E-F-G. This implies that the predicted foundation stiffness with API *p-y* curves is too low after reversal at points E and F. The loop E-F-G does not enclose any area, which means that no hysteretic damping is generated. The same discrepancies are found while analysing case 2.

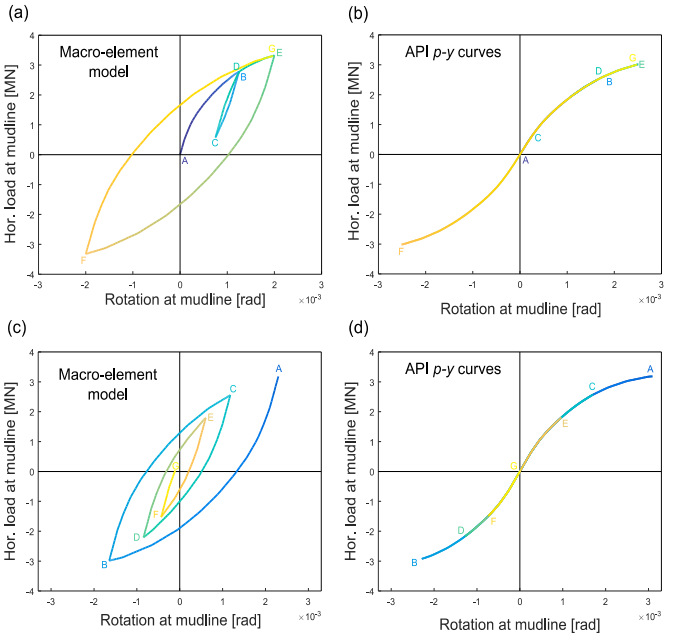

Fig. 10. Horizontal load-rotation response at mudline for two examples computed with different foundation models: (a) case 1 computed with the macro-element model calibrated by FEA; (b) case 1 computed with API *p-y* curves; (c) case 2 computed with the macro-element model calibrated by FEA; (d) case 2 computed with API *p-y* curves.

5. Discussion and Conclusion

The paper introduces a new foundation model for integrated analyses of monopile-based OWTs. The model can reproduce the non-linear load-displacement response and the hysteretic behaviour observed for piled foundations. The model follows the macro-element concept, where the response of the foundation and the surrounding soil is reduced to a force–displacement relation in one point at an interface, in this case at mudline. The model formulation is based on trends observed in FEA of the soil and the foundation. In the FEA, the soil response is reproduced with the NGI-ADP, a constitutive model which mimics the behaviour of cohesive soils. From the FEA, it is found that the relation between the forces (horizontal load and overturning moment) and the plastic displacements (horizontal displacement and rotation) at mudline could be simplified from a 2 to a 1 degree of freedom system by translating the formulation to a point below mudline, denoted the plastic decoupling point. The FEA indicated that for moderate load levels, a fixed plastic decoupling point can be assumed in the macro-element formulation. This simplifies the model but it also limits the valid range since the plastic decoupling point will vary for higher load levels. More FEA for specific foundation dimensions and soil types at the relevant load levels are needed to evaluate the impact of this assumption.

The greatest advantage of the model is its simplicity. The intuitive physical analogue makes the model easy to understand, to calibrate and to implement in integrated analyses. The model calibration is done by means of FEA of the soil and the foundation.

In this way, the accuracy of the FEA can be combined with computationally efficient macro-element models while modelling the foundation response in integrated analyses of OWT. The macro-element model is being implemented in an OWT load simulation code, *3DFloat,* via a *dll* interface.

The macro-element model performance has been compared with the response of a pile calculated by means of API *p-y* curves for time histories representative for a monopile supporting an OWT. In contrast to the API *p-y* curves, the improved model can reproduce different foundation stiffness for unloading and reloading and foundation damping depending on the loading history, which is observed in real pile behaviour. A more realistic foundation modelling will lead to more accurate predicted loads, reduced uncertainties in the estimated fatigue lifetime and therefore reduced risk in the design.

Acknowledgements

The financial support by the Norwegian Research Council through project *Reducing cost of offshore wind by integrated structural and geotechnical design (REDWIN)*, Grant No. 243984, is gratefully acknowledged. The constructive comments and suggestions given by Sebastian Schafhirt are also appreciated.

References

[1] F. Vorpahl, H. Schwarze, T. Fischer, M. Seidel, J. Jonkman. Offshore wind turbine environment, loads, simulation, and design. Wiley Interdisciplinary Reviews: Energy and Environment; 2013; 548-570.
[2] Det Norske Veritas. Design of offshore wind turbine structures. In Det Norske Veritas; 2014.
[3] S. Aasen, A.M. Page, K.S. Skau, T.A. Nygaard. Effect of the Foundation Modelling on the Fatigue Lifetime of a Monopile-based Offshore Wind Turbine. Manuscript submitted for publication.
[4] B. Byrne, G. Houlsby. Foundations for offshore wind turbines. Philosophical Transactions of the Royal Society of London A: Mathematical, Physical and Engineering Sciences; 2003; 361:2909-2930.
[5] L. Andersen. Assessment of lumped-parameter models for rigid footings. Computers & Structures; 2010; 88:1333-1347.
[6] D. Kallehave, C.L. Thilsted, A. Troya. Observed variations of monopile foundation stiffness. In Frontiers in Offshore Geotechnics III, Oslo; 2015. p. 557-562.
[7] M. Damgaard, L.B. Ibsen, L.V. Andersen, J. Andersen. Cross-wind modal properties of offshore wind turbines identified by full scale testing. Journal of Wind Engineering and Industrial Aerodynamics; 2013; 116:94-108.
[8] R. Shirzadeh, C. Devriendt, M.A. Bidakhvidi, P. Guillaume. Experimental and computational damping estimation of an offshore wind turbine on a monopile foundation. Journal of Wind Engineering and Industrial Aerodynamics; 2013; 120:96-106.
[9] N.J. Tarp-Johansen, L. Andersen, E.D. Christensen, C. Mørch, S. Frandsen. Comparing sources of damping of cross-wind motion. In European Offshore Wind 2009: Conference & Exhibition: 14-16 September, Stockholm, Sweden. The European Wind Energy Association; 2009.
[10] W. Versteijlen, A. Metrikine, J. Hoving, E. Smidt, W. De Vries. Estimation of the vibration decrement of an offshore wind turbine support structure caused by its interaction with soil. In: Proceedings of the EWEA Offshore 2011 Conference, Amsterdam, The Netherlands, 29 November-1 December 2011, European Wind Energy Association; 2011.
[11] API. Recommended Practice for Planning, Designing and Constructing Fixed Offshore Platforms - Working Stress Design. In American Petroleum Institute; 2011.
[12] P. Doherty, K. Gavin. Laterally loaded monopile design for offshore wind farms. Proceedings of the Institution of Civil Engineers; 2011; 165:7-17.
[13] K. Lesny. Foundations for Offshore Wind Turbines: Tools for Planning and Desing. VGE-Verlag; 2010.
[14] L.C. Reese, W.R. Cox, F.D. Koop. Field testing and analysis of laterally loaded piles om stiff clay. In Offshore Technology Conference; 1975.
[15] B. Byrne, R. McAdam, H. Burd, G. Houlsby, C. Martin, L. Zdravković, D. Taborda, D. Potts, R. Jardine, M. Sideri. New design methods for large diameter piles under lateral loading for offshore wind applications. In Frontiers in Offshore Geotechnics III, Oslo; 2015. p. 705-710.
[16] D. Kallehave, B.W. Byrne, C.L. Thilsted, K.K. Mikkelsen. Optimization of monopiles for offshore wind turbines. Philosophical Transactions of the Royal Society of London A: Mathematical, Physical and Engineering Sciences; 2015; 373.
[17] M.B. Zaaijer. Foundation modelling to assess dynamic behaviour of offshore wind turbines. Applied Ocean Research; 2006; 28:45-57.
[18] T. Hald, C. Mørch, L. Jensen, C. Bakmar, K. Ahle. Revisiting monopile design using py curves. Results from full scale measurements on Horns Rev. In Proceedings of European Offshore Wind 2009 Conference; 2009.
[19] O. Hededal, R.T. Klinkvort. A new elasto-plastic spring element for cyclic loading of piles using the py curve concept. In Numerical Methods in Geotechnical Engineering; 2010; 883-888.
[20] G. Masing. Eigenspannungen und verfestigung beim messing. In Proceedings of the 2nd International Congress of Applied Mechanics; 1926. p. 332-335.
[21] W. Beuckelaers. Fatigue life calculation of monopiles for offshore wind turbines using a kinematic hardening soil model. In Ground Engineering; 2015. p. 26-29.
[22] K. Roscoe, A. Schofield. The stability of short pier foundations in sand. British Welding Journal; 1956; 3: 343-354.
[23] R. Butterfield, G. Gottardi. A complete three-dimensional failure envelope for shallow footings on sand. Géotechnique; 1994; 44:181-184.
[24] C.M. Martin. Physical and numerical modelling of offshore foundations under combined loads. PhD Thesis, University of Oxford; 1994.
[25] L. Nguyen-Sy. The theoretical modelling of circular shallow foundation for offshore wind turbines. PhD Thesis, University of Oxford; 2007.
[26] L. Nguyen-Sy, G.T. Houlsby. The theoretical modelling of a suction caisson foundation using hyperplasticity theory. In Frontiers in Offshore Geotechnics II, Perth; 2005. p. 417.
[27] A. Correia. A pile-head macro-element approach to seismic design of monoshaft-supported bridges. PhD Thesis, European School for Advanced Studies in Reduction of Seismic Risk (ROSE School), Pavia, Italy; 2011.
[28] Z. Li, P. Kotronis, S. Escoffier, C. Tamagnini. A hypoplastic macroelement for single vertical piles in sand subject to three-dimensional loading conditions. Acta Geotechnica; 2016; 11:373-390.
[29] V. Krathe, A. Kaynia. Implementation of a non-linear foundation model for soil-structure interaction analysis of offshore wind turbines in FAST. Wind Energy; 2016.
[30] G. Grimstad, L. Andresen, H.P. Jostad. NGI-ADP: Anisotropic shear strength model for clay. International Journal for Numerical and Analytical Methods in Geomechanics; 2012; 36:483-497.
[31] W.D. Iwan. On a class of models for the yielding behavior of continuous and composite systems. Journal of Applied Mechanics; 1967; 34:612-617.
[32] T.A. Nygaard, J. De Vaal, F. Pierella, L. Oggiano, R. Stenbro. Development, Verification and Validation of 3DFloat; Aero-servo-hydro-elastic Computations of Offshore Structures. Energy Procedia; 2016; 94:425-433.
[33] G. Gazetas. Foundation vibrations. Foundation engineering handbook. Springer; 1991. p. 553-593.
[34] M.F. Randolph. The response of flexible piles to lateral loading. Geotechnique; 1981; 31:247-259.
[35] K.H. Andersen. Cyclic soil parameters for offshore foundation design. In Frontiers in Offshore Geotechnics III, Oslo; 2015. p. 5.
[36] A. Kaynia, K. Andersen. Development of nonlinear foundation springs for dynamic analysis of platforms. In Frontiers in Offshore Geotechnics III, Oslo; 2015.
[37] K.S. Skau, H.P. Jostad. Application of the NGI-Procedure for Design of Bucket Foundations for Offshore Wind Turbines. In the Twenty-fourth International Ocean and Polar Engineering Conference. International Society of Offshore and Polar Engineers; 2014.